Monthly Notices of the ROYAL ASTRONOMICAL SOCIETY

MNRAS **464,** 850–862 (2017) doi:10.1093/mnras/stw2345
Advance Access publication 2016 September 15

Zodiacal exoplanets in time (ZEIT) – II. A 'super-Earth' orbiting a young K dwarf in the Pleiades Neighbourhood

E. Gaidos,[1,2★] A. W. Mann,[3†] A. Rizzuto,[3] L. Nofi,[4] G. Mace,[3] A. Vanderburg,[5] G. Feiden,[6] N. Narita,[7,8,9,10] Y. Takeda,[9] T. M. Esposito,[11] R. J. De Rosa,[11] M. Ansdell,[4] T. Hirano,[12] J. R. Graham,[11] A. Kraus[3] and D. Jaffe[3]

[1]*Department of Geology and Geophysics, University of Hawaii at Mānoa, Honolulu, HI 96822, USA*
[2]*Visiting Scientist, Center for Space and Habitability, University of Bern, CH-3012, Switzerland*
[3]*Department of Astronomy, University of Texas at Austin, Austin, TX 78712, USA*
[4]*Institute for Astronomy, University of Hawaii at Mānoa, HI 96822, USA*
[5]*Harvard-Smithsonian Center for Astrophysics, Cambridge, MA 02138, USA*
[6]*Department of Physics and Astronomy, Uppsala University, SE-751-20 Uppsalla, Sweden*
[7]*Department of Astronomy, The University of Tokyo, Bunkyo-ku, 113-0038 Tokyo, Japan*
[8]*Astrobiology Center, National Institutes of Natural Sciences, Mitaka, 181-8588 Tokyo, Japan*
[9]*National Astronomical Observatory of Japan, Mitaka, 181-8588 Tokyo, Japan*
[10]*SOKENDAI (The Graduate University for Advanced Studies), Mitaka, 181-8588 Tokyo, Japan*
[11]*Department of Astronomy, University of California at Berkeley, Berkeley, CA 94720, USA*
[12]*Department of Earth and Planetary Sciences, Tokyo Institute of Technology, Meguro-ku, 152-8551 Tokyo, Japan*

Accepted 2016 September 14. Received 2016 September 10; in original form 2016 June 18

ABSTRACT

We describe a 'super-Earth'-size (2.30 ± 0.16 $R_\oplus$) planet transiting an early K-type dwarf star in the Campaign 4 field observed by the *K2* mission. The host star, EPIC 210363145, was identified as a candidate member of the approximately 120 Myr-old Pleiades cluster based on its kinematics and photometric distance. It is rotationally variable and exhibits near-ultraviolet emission consistent with a Pleiades age, but its rotational period is ≈20 d and its spectrum contains no Hα emission nor the Li I absorption expected of Pleiades K dwarfs. Instead, the star is probably an interloper that is unaffiliated with the cluster, but younger ($\lesssim$1.3 Gyr) than the typical field dwarf. We ruled out a false positive transit signal produced by confusion with a background eclipsing binary by adaptive optics imaging and a statistical calculation. Doppler radial velocity measurements limit the companion mass to <2 times that of Jupiter. Screening of the light curves of 1014 potential Pleiades candidate stars uncovered no additional planets. An injection-and-recovery experiment using the *K2* Pleiades light curves with simulated planets, assuming a planet population like that in the *Kepler* prime field, predicts only 0.8–1.8 detections (versus ∼20 in an equivalent *Kepler* sample). The absence of Pleiades planet detections can be attributed to the much shorter monitoring time of *K2* (80 d versus 4 yr), increased measurement noise due to spacecraft motion, and the intrinsic noisiness of the stars.

Key words: planets and satellites: general – stars: low-mass – planetary systems – open clusters and associations: individual: Pleiades.

1 INTRODUCTION

Since antiquity, the Pleiades cluster has been used to mark the passage of time. The name may derive from the ancient Greek word $\pi\lambda\epsilon\omega$ ('to sail') because the constellation's helical rising marked the advent of fair weather sailing in the Mediterranean.[1] The appearance of the Pleiades (Makali'i) in the evening sky begins Makahiki, the Hawaiian harvest season.

Scientific studies of the Pleiades revealed it to be a nearby cluster of very young (e.g. 112 ± 5 million years (Myr); Dahm 2015) stars and this object serves studies of star formation, stellar

★ E-mail: gaidos@hawaii.edu
† NASA Hubble Postdoctoral Fellow

[1] The helical rising of Pleiades currently happens the first week of June but due to the precession of the equinoxes, it occurred mid-spring in Iron Age Europe.

© 2016 The Authors
Published by Oxford University Press on behalf of the Royal Astronomical Society

evolution, stellar dynamics, ultracool stars and planetary-mass bodies (Casewell et al. 2007; Zapatero Osorio et al. 2014). It provides a (controversial) calibration tie-point for distance measurements (Melis et al. 2014). Observations of the Pleiades, and other young clusters are also ways to identify and study planets younger than those in surveys of the field such as *Kepler* . Many important events probably occur in the first few hundred Myr of planetary systems, e.g. thermal and radius evolution of gas- and ice-giant planets (Fortney et al. 2011; Guillot & Gautier 2014), the heating and escape of planetary atmospheres driven by elevated ultraviolet (UV) emission from the active host star (Tian et al. 2005), planet migration, orbital resonance crossing (Gomes et al. 2005; Thommes, Nagasawa & Lin 2008), and collisions (Volk & Gladman 2015).

Comparisons of the planet populations in young clusters such as the Pleiades with older field dwarfs can elucidate such processes. For example, a higher occurrence of planets around young cluster stars compared to field stars would point to subsequent photoevaporation of hydrogen envelopes and decreasing planet radii that renders older planets more difficult to detect. A lower occurrence of planets could be explained by subsequent inward migration of planets to more detectable orbits.

Because of Malmquist (limiting magnitude) bias and the Galactic latitude ($b \sim 13^\circ$) of the field of the *Kepler* 'prime' mission, its target stars are primarily middle-aged dwarfs and evolved (subgiant) stars (Gaidos & Mann 2013). The successor *K2* mission is observing fields near the ecliptic place which include several young clusters, OB associations, and star-forming regions, i.e. the Hyades, Pleiades, Praesepe, ρ Ophiuchus, Upper Scorpius, and Taurus clusters.

The Zodiacal exoplanets in time project is confirming and characterizing candidate transiting planets detected by *K2* around young cluster stars. We previously reported a Neptune-size planet around an ∼650 Myr-old Hyades star (Mann et al. 2016b; see also David et al. 2016)) and a 'super-Neptune' around an ∼11 Myr-old member of the Upper Scorpius OB association (Mann et al. 2016a). Here we report the discovery and validation of an ≈2.3-Earth-radius ($R_\oplus$) 'super-Earth'-size planet on a 8.2-d orbit around EPIC 210363145, a K-type dwarf star in the vicinity of the Pleiades.[2] This star was selected on the basis of multiple Guest Observer target proposals for Campaign 4, which includes both the Pleiades and a portion of the Hyades cluster. In Section 2, we describe the *K2* photometry of EPIC 210363145 and our follow-up spectroscopy and imaging. In Section 3, we describe our analysis and derivation of the host star parameters; in Section 4, that of the planet parameters. In Section 5, we discuss the ambiguous nature of EPIC 210363145 and the implications of our planet detections – or lack thereof – for the planet population in the Pleiades cluster.

2 OBSERVATIONS AND DATA REDUCTION

2.1 *Kepler* photometry

Light curves processed by the Vanderburg & Johnson (2014) pipeline were downloaded from the STScI Mikulski Archive for Space Telescopes (MAST) data base and subjected to secondary treatment. Light curves were normalized and a Lomb–Scargle periodogram power spectrum (Scargle 1982) was generated. To remove periodic variability due to spots and rotation and enhance the detection of transits, significant peaks were identified and any signal with a period within 10 per cent of these peaks was filtered from a fast Fourier transform. The light curve was then further filtered by a median filter with a sliding window of 1 d, a robust standard deviation was calculated using Tukey's biweight function (Tukey 1977) and anomalous positive excursions $>3\sigma$ were removed. A linear regression of the flux versus motion along the 'arc' of the *K2* pointing error (Vanderburg & Johnson 2014) was re-performed and subtracted.

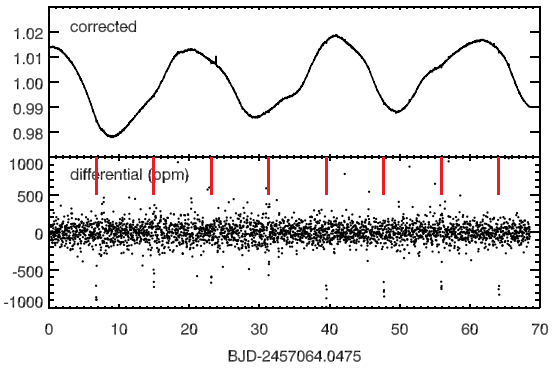

Figure 1. Top: Vanderburg pipeline-corrected and normalized light curve of EPIC 210363145, showing the ∼3 per cent peak-to-peak rotational variability. Bottom: differential light curve constructed by robustly fitting a quadratic to the corrected data within a moving 0.5-d window centred on each data point and subtracting the predicted value at that point. Red fiducials mark the transits of the planet described here.

To identify potential transiting planet signals, an initial box-least-squares (BLS) search (Kovács, Zucker & Mazeh 2002) was performed. The search was performed over a period range of 1–25 d and with a box width (transit duration) that ranged from 0.5 to 2 times the nominal transit duration for the estimated density of the host star, a zero impact parameter, and a circular orbit. Significant (false alarm probability <0.01) peaks in the initial BLS power spectrum were identified and an individual BLS search with a finer mesh of period and duration values was performed around each peak. A signal-to-noise ratio (SNR) was calculated based on the in- versus out-of-transit points and a criterion of SNR > 7 applied. An F-test (ratio of χ^2 values) was performed to evaluate whether the transit model was a significantly better fit to the data than the no-transit (flat) model. Finally, the mean ratio of odd- to even-numbered transits, an important indicator of false positives produced by eclipsing binaries, was calculated. Fig. 1 shows the Vanderburg & Johnson (2014)-corrected light curve and a differential version exhibiting the individual transits.

We ran an additional BLS search with a different handling of stellar variability. We first applied a median filter with a window of 2.5 h to remove even rapid (<6 h) rotation. We removed anomalous points as before, then fed the filtered and flatted light curve into the BLS search. This short median window smooths out stellar variability but also erases or weakens shallow and/or long duration transits. If no significant peak was identified in the BLS, we widened the window in increments of 0.25 h up to 1 d. If a significant signal was identified in the BLS, we re-fit the stellar variability, interpolating over the transits, and fit the resulting transit using Levenberg–Markwardt least-squares minimization (Markwardt 2009). Because this method produces a larger number of false positives, we required the transit signal to be consistent with a non-grazing transit (with a flat bottom), a planetary size, have a duration and period inconsistent with the stellar variability, and be symmetric about the mid-point, in addition to the odd-even test performed above.

[2] Crossfield et al. (2016) also reported this object.

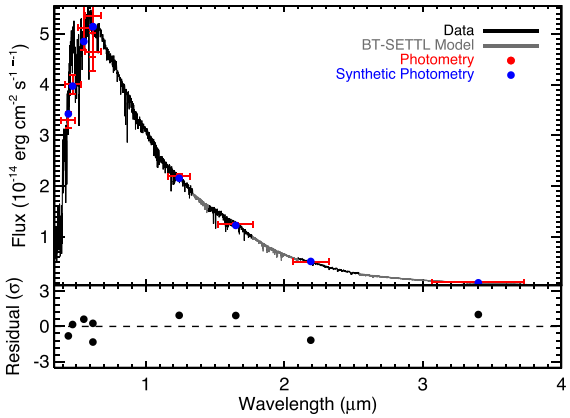

Figure 2. Flux-calibrated spectrum of EPIC 210363145, created by combining observed visible (SNIFS) and near-infrared (SpeX) spectra, filling unobservable gaps with the best-fitting model spectrum, and constructing synthetic photometry from the composite spectrum to compare to the observations.

2.2 Low-resolution spectroscopy

A moderate resolution ($R \approx 1000$) visible-wavelength (3200–9700 Å) spectrum was obtained on UT 17 January 2016 using the SuperNova Integral Field Spectrograph (SNIFS; Aldering et al. 2002; Lantz et al. 2004) on the UH 2.2 m telescope on Mauna Kea. The integration time was 110 sec and the observation airmass was 1.01. Details of the spectrograph and data reduction are given in Gaidos et al. (2014) and Mann et al. (2015).

A near-infrared (*JHK*, 0.8-2.4μm) spectrum was obtained with the SpeX spectrograh on the NASA Infrared Telescope Facility (IRTF) on Mauna Kea (Rayner et al. 2003). Extraction and calibration of this spectrum was performed using the SpeXTool package (Cushing, Vacca & Rayner 2004) and corrected for telluric absorption using the spectrum of an A0 star as described in Vacca, Cushing & Rayner (2003). The SNIFS and SpeX spectra were combined and flux-calibrated (Fig. 2) using the available photometry and the methods described in Mann et al. (2015) and filter profiles and zero-points from Mann & von Braun (2015).

2.3 High-resolution spectroscopy

High-resolution ($R \approx 65\,000$) visible-wavelength spectra were obtained on UT 2016 January 26 and 29 with the High Dispersion Spectrograph (HDS) on the *Subaru* telescope on Mauna Kea. The airmass of the observations was 1.09 and 1.02, respectively. Two different setups were used: the standard 'Ub' setup covering 2980–3700 and 3820–4580 Å on two different CCDs, and the standard 'Ra' setup covering 5110–6310 and 6580–7790 Å. A 0.8 arcsec slit giving a resolution $R = 45\,000$ was used for both modes. Total integration times were 3600 and 900 s with the Ub and Ra settings, respectively. Flat-fields were obtained using a quartz lamp and wavelength calibration was provided by spectra of a Th–Ar arc lamp. Reduction (dark removal, flat-fielding, order extraction, wavelength calibration, and blaze correction) used IRAF routines developed at the National Astronomical Observatory of Japan (NAOJ) and analysis was performed with custom GDL scripts.

High-resolution NIR spectra were taken at three epochs (2016 January 4, February 3 and 4) with the Immersion Grating Infrared Spectrometer (IGRINS; Park et al. 2014) attached to the 2.7 m Harlan J. Smith Telescope at Mcdonald Observatory. IGRINS is a fixed-format, high-resolution ($R \simeq 45\,000$) NIR spectrograph with simultaneous coverage from 1.5 to 2.5 μm. An A0V telluric standard was taken before or after the target each epoch. Th–Ar and U–Ne as well as dark and flat-field calibration data were taken at the start of each night. IGRINS spectra were reduced with the IGRINS pipeline package (https://github.com/igrins/plp; Lee 2015). This included bias, flat, and dark field corrections, and extraction of the 1D spectra of both the A0V standard and target. We used the A0V spectra to correct telluric lines following the method outlined in Vacca et al. (2003). Pre-telluric corrected spectra of the target were retained and used to improve the wavelength solution and provide a zero-point for the radial velocities (RVs). RVs for each IGRINS epoch were derived following the procedure outlined in Mann et al. (2016b).

2.4 High-resolution imaging

We obtained adaptive optics imaging through the K' filter ($\lambda_c = 2.124$ μm, $\Delta\lambda = 0.31$ μm) with the Near-Infrared Camera (NIRC2) at the Keck-2 telescope on Mauna Kea during the nights of UT 18 January and 18 March 2016. The narrow camera (pixel scale of 0.01 arcsec) was used for both sets of observations. In addition to normal AO imaging, data for non-redundant aperture masking interferometry (NRM) (Tuthill, Monnier & Danchi 2000) were obtained with the 9-hole mask on the second night. Images were processed using a custom PYTHON pipeline: images were linearized (Metchev & Hillenbrand 2009), dark-subtracted, flattened, sky-subtracted, and co-added. A cutout ∼1.5 arcsec across, centred on the star, was made and inserted back into the processed image as a simulated companion. The routine generated a contrast curve by decreasing the brightness and angular separation of the simulated companion with respect to the primary, until the limits of detection (3.5σ) are reached.

The data obtained for non-redundant aperture masking are essentially a collection of interferograms from pairs of apertures created in the pupil plane of the Keck-2 telescope. Details of the data reduction are given in the appendix of Kraus et al. (2008). Non-common path errors introduced by the atmospheric and optical aberrations were removed using the complex triple product, or closure-phase. In the case of EPIC 210363145, the observations were paired with those of nearby EPIC 210894022. Binary system profiles were fit to the closure phases to calculate contrast limits. No additional sources were detected and the combined AO imaging+NRM detection limit contrast curve is plotted in Fig. 3.

3 ANALYSIS: THE HOST STAR

3.1 Pleiades candidate selection

We identified members of the Pleiades cluster using kinematic and photometric information for the candidate stars. Proper motions were gathered from the UCAC4 (Zacharias et al. 2013) and PPMXL (Róser, Demleitner & Schilbach 2010) catalogs for all objects in the Pleiades field, and combined with our own proper motion catalogue generated from the USNO-B (Monet et al. 2003), SDSS, and 2MASS (Skrutskie et al. 2006) catalogs as described in Kraus et al. (2014). We also calculated photometric distances for both a field main sequence and a Pleiades age (∼100 Myr) Padova isochrone (Bressan et al. 2012) using APASS *BV* (Henden et al. 2012) and 2MASS *JK* photometry where available, for each candidate member. We then calculated probabilities of membership in the Pleiades according to the Bayesian method described in Rizzuto, Ireland & Robertson (2011) and Rizzuto, Ireland & Kraus (2015)

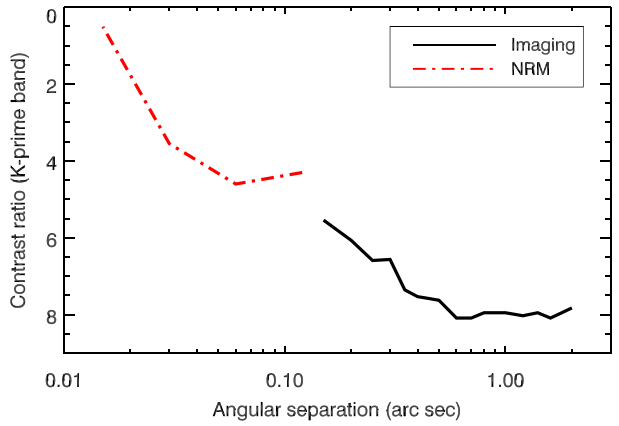

Figure 3. Detection limits (99.9 per cent) for sources close to EPIC 210363145 placed by AO observations with Keck-2, reported as a magnitude contrast in the K' passband of the NIRC2 detector. Limits based on non-redundant aperture mapping are plotted as the red dash–dotted line.

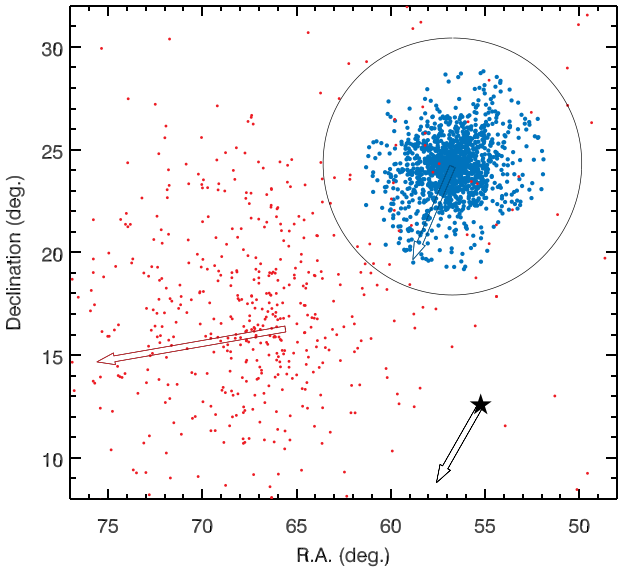

Figure 4. Location of EPIC 210363145 (star) with respect to the Pleiades (blue) and Hyades (red) clusters. Arrows show the relative magnitude and direction of proper motions. Pleiades stars are from the catalogue of Stauffer et al. (2007) and Hyades stars are from the catalogue of Röser et al. (2011). The 13.1-pc tidal radius of the Pleiades cluster estimated by Adams et al. (2001) is plotted as a circle.

and the Pleiades kinematics of van Leeuwen (2009). With the radial velocity (RV) from our IGRINS spectrum ($7.35 \pm 0.20\,\mathrm{km\,s^{-1}}$), EPIC 210363145 was assigned a 99.6 per cent probability of membership in the Pleiades as opposed to a field star.

3.2 Kinematics and distance

EPIC 210363145 lies at a projected distance of 11.°7 (≈28 pc) from the cluster centroid (Fig. 4) and well outside the tidal radius of 13 pc (Adams et al. 2001). No parallax is available for EPIC 210363145, thus we estimated a distance assuming it is a Pleiades member and finding the distance which maximizes the probability that its space motions would be that of a cluster member. We adopted the *Hipparcos*-based Pleiades *UVW* values and uncertainties of van Leeuwen (2009) (-6.7 ± 0.9, -25.0 ± 0.5, $-12.8 \pm 0.5\,\mathrm{km\,s^{-1}}$), and a Gaussian isotropic velocity dispersion with $\sigma = 0.6\,\mathrm{km\,s^{-1}}$ (Geffert, Kuemmel & Schmidt 1995; Li & Junliang 1999; Makarov & Robichon 2001). We repeated the calculations, altering the input parameters according to normal distribution with the published standard errors and summing the distributions. The resulting distance posterior has a mean value of 125 pc with a standard deviation of 5 pc. This is (marginally) smaller than the very long baseline interferometry (VLBI) distance to the Pleiades (136.2 ± 1.2 pc; Melis et al. 2014). The most probable space motions corresponding to this kinematic distance are $(U,V,W) = (-5.5,-27.5,-9.2)$ $\mathrm{km\,s^{-1}}$ and the expectation of the velocity offset from the nominal cluster motion is $2\,\mathrm{km\,s^{-1}}$.

3.3 Stellar rotation

The *K2* light curve of EPIC 210363145 shows pronounced (∼3 per cent peak-to-peak) variability with a period of ≈20 d that we attribute to rotation and star-spots. We performed a systematic determination of the rotation periods of EPIC 210363145 as well as our entire sample of Pleiades candidate members, following the procedure outlined by McQuillan, Aigrain & Mazeh (2013). The light curves generated by the Vanderburg & Johnson (2014) pipeline were downloaded from the STScI archive, normalized by the median value, and detrended with a robust fit of a quadratic with time. Each detrended light curve was then interpolated on to a regular grid set by the *Kepler* long cadence of 29.4 min. An autocorrelation function (ACF) was computed, and median-smoothed with an interval of 5.5 h (11 points). Maxima and minima were identified and the second and third maxima were inspected (the first maximum is at zero lag). Because rotational variability sometimes contains a higher harmonic, the second, rather than the first peak in the ACF may be the actual period – this is usually the larger of the two extrema. A Gaussian function was fit to the ACF in the vicinity of this maximum to obtain a refined estimate for the period. The ACF-based rotational period of EPIC 210363145 was found to be 19.8 d. The highest peak in the Lomb–Scargle periodogram is at 20.0 d. We derived a relation for the uncertainty in an ACF-based period σ_P by evaluating the ACF of a signal with a Gaussian power spectrum with a width of $1/\sigma_\mathrm{P}$. The ACF of an infinite time series of this signal is a cosine modulated by a decaying exponential, and σ_P is related to the height H of the (first) peak in the ACF by

$$\sigma_\mathrm{P} \approx P\sqrt{-\log H/(2\pi^2)}. \quad (1)$$

For the light curve of EPIC 210363145, we find $H = 0.65$ and $\sigma_\mathrm{P} = 2.9$ d. The surprisingly large uncertainty is most likely due to the rapidly changing shape of the light curve as a result of differential rotation of spots.

We successfully determined rotational periods for 383 other Pleiades candidates following the same method. The rotational period and $r - J$ colour of these Pleiades candidates are plotted in Fig. 5, with EPIC 210363145 indicated as the star, and points are colour-coded according to membership probability. Equivalent stellar masses on a 120-Myr solar-metallicity isochrone, calculated using the Dartmouth Stellar Evolution Program (Dotter et al. 2008), are also shown on the top axis. Pleiades candidates exhibit the established bifurcation between the 'slow' (few days) and 'fast' (<1 d) rotators among K dwarfs (Queloz et al. 1998; Hartman et al. 2010), as well as a more continuous dispersion among late K dwarfs and M dwarfs (see also Rebull et al. 2016). EPIC 210363145 occupies a zone occupied by more slowly rotating (20–30 d) stars with a wider range of membership probabilities.

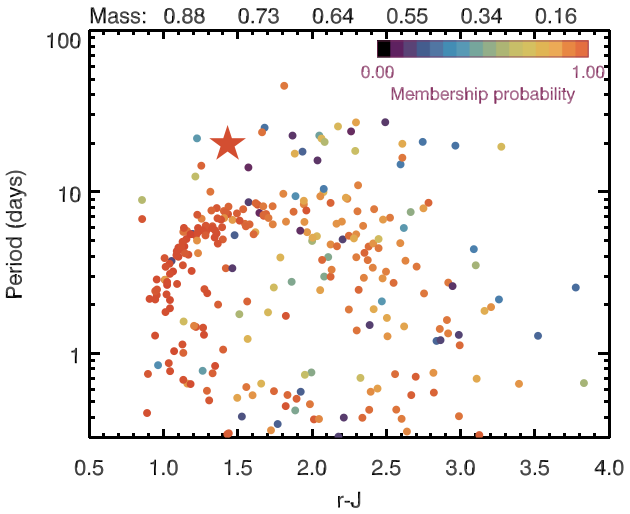

Figure 5. Rotation periods of our 383 Pleiades candidates, including EPIC 210363145 (star), versus *r*-*J* colour. Rotation periods were determined using the autocorrelation function following the procedure of (McQuillan et al. 2013). Membership probability is indicated by the colours of the points (see colorbar). Equivalent stellar masses (solar units) estimated from a 120-Myr solar-metallicity isochrone from the Dartmouth Stellar Evolution Program (Dotter et al. 2008) are reported for some $r-J$ colours.

The light curve of EPIC 210363145 (Fig. 1) and its changing shape (i.e. the rising secondary peak) is reminiscent of that of KIC 1869793, examined by Reinhold, Reiners & Basri (2013), which has a similar $B - V$ colour but a longer rotation period (26.2 d). Reinhold et al. (2013) interpret this as a manifestation of migrating spots and differential rotation.

3.4 Stellar activity and lithium

Neither the SNIFS or HDS spectrum of EPIC 210363145 show evidence of Hα in emission; instead, as is characteristic of K dwarfs, it is in absorption (Fig. 6), with an equivalent width (EW) of -1.08 ± 0.31 Å measured from the SNIFS spectrum. We compared the spectrum of EPIC 210363145 in the vicinity of the Hα, Ca II infrared triplet, and Ca II H and K lines with those of three inactive K dwarfs with similar effective temperatures accurately established by combining interferometrically measured angular radii and bolometric fluxes (Boyajian et al. 2012, 2015). The comparison (Fig. 6) shows that the spectra are almost indistinguishable and that of EPIC 210363145 shows no filling of the cores of these lines as expected for an active, Pleiades-age star. The Hα EW of EPIC 210363145 is indistinguishable from the three stars (-0.81, -0.81, -0.89 and -0.89, ± 0.01 Å), and this similarity is not sensitive to the exact $T_{\rm eff}$.

EPIC 210363145 has a counterpart near-ultraviolet (NUV, ~2300 Å) source in the *GALEX* DR-5 catalogue (Bianchi et al. 2011) with an AB magnitude of 19.96 ± 0.10. Adopting extinction coefficients $R(\mathrm{NUV}) = 7.24$, $R(V) = 3.2$, and $R(J) = 0.72$ (Yuan, Liu & Xiang 2013) and an extinction of $A_V = 0.12$ (Guthrie 1987), the intrinsic NUV colour should be $m_{\rm NUV} - J = 8.79$. This places it directly on the locus of AB Doradus stars in the NUV$-J$ versus $J - K_s$ colour–colour diagram constructed by Findeisen, Hillenbrand & Soderblom (2011). The age of the AB Dor moving group is probably similar to that of the Pleiades (Luhman, Stauffer & Mamajek 2005; McCarthy & Wilhelm 2014). We identified NUV source counterparts for 40 other Pleiades candidates from the *GALEX* All-sky Imaging Survey (AIS) and these are plotted versus

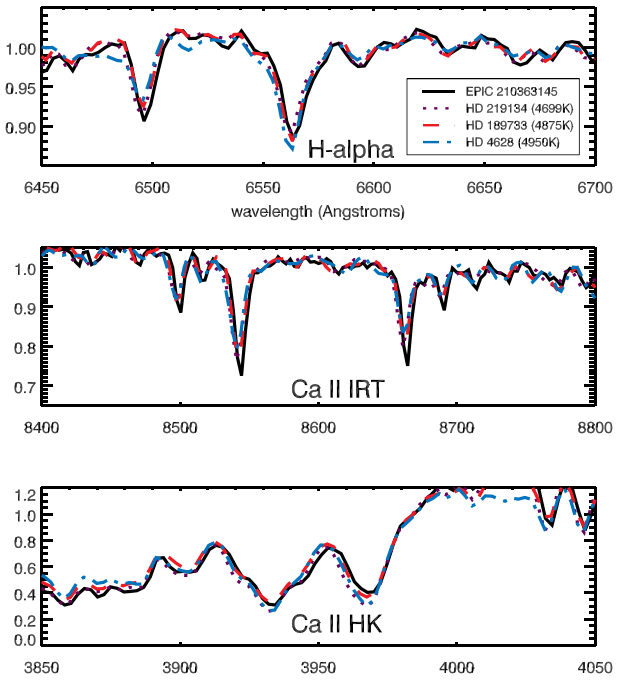

Figure 6. SNIFS spectrum of EPIC 210363145 in the vicinity of the (top) 6563 Å Balmer α line of H I, (middle) the infrared triplet of Ca II, and (bottom) the H and K lines of Ca II, emission in any of which is an indication of magnetic activity on dwarf stars. In each region the spectrum is compared to that of three K dwarf stars with similar effective temperatures obtained by combining interferometrically measured angular radii and bolometric fluxes. Spectra are normalized by median values and wavelengths are presented in the observed frame, in air; offsets are not removed to allow spectra to be distinguished. Note the difference in scales between plots.

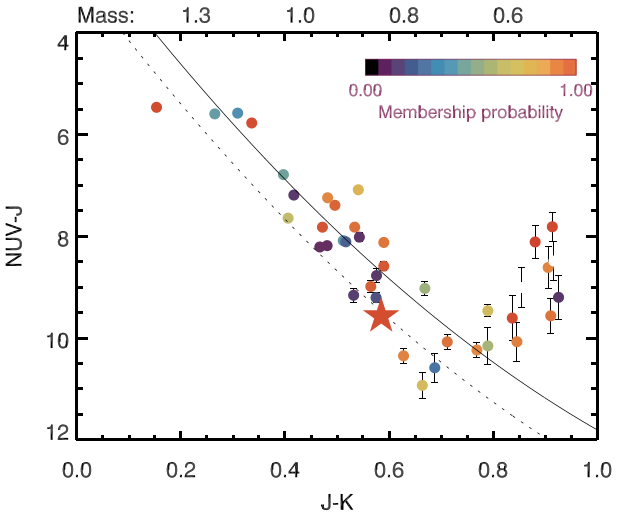

Figure 7. Near-ultraviolet NUV$-J$ versus $J-K$ colours of Pleiades candidates, with EPIC 210363145 plotted as the star. Equivalent stellar masses (solar units) based on a 120-Myr solar-metallicity DSEP isochrone are given for some colours. The solid curve is the 120 Myr-locus predicted by the Findeisen et al. (2011) relation based on observations of nearby comoving groups, assuming zero extinction. The dashed curve is the same but assumes $A_V = 0.12$ and the extinction coefficients of Yuan et al. (2013).

$J-K$ in Fig. 7. Many Pleiades stars with $J-K<0.8$ fall along a locus that is consistent with the prediction of Findeisen et al. (2011) for an age of 120 Myr based on observations of nearby comoving groups. EPIC 210363145 and some other stars fall below that curve, but can be reconciled assuming Pleiades-like extinction. In contrast, detected M dwarfs ($J-K>0.8$) are more UV-luminous than the Findeisen et al. (2011) prediction. The locus is not an artefact of the detection limit of the AIS. For a typical limiting $m_{\rm NUV}\approx21$ (Bianchi 2014), the limiting NUV$-J$ for the Pleiades is $\geq$15.

There is no significant absorption at the 6708 Å resonant doubled of Li I in the spectrum of EPIC 210363145. We placed an upper limit of 5 mÅ on the EW. Using the curves of growth calculated by (Lind, Asplund & Barklem 2009), this EW corresponds approximately to a limit on lithium abundance (with respect to the solar value) of $\log A({\rm Li})<0.4$ to 0.5 ($T_{\rm eff}=5000$ K, $\log g=4.5$) or <-0.30 to -0.1 ($T_{\rm eff}=4500$ K, $\log g=4.5$), depending on whether the assumption of local thermodynamic equilibrium holds. This is below the nominal distribution for Pleiades stars (e.g. Somers & Pinsonneault 2015).

3.5 Stellar parameters

Because robust stellar parameters are both important and potentially challenging for young systems, we made multiple, independent estimates for EPIC 210363145 based on photometry or spectroscopy to check consistency. We first estimated $T_{\rm eff}$ based on $B-V$ and $V-K$ colours with BV magnitudes from Data Release 9 of the APASS survey and K magnitudes from 2MASS, and the $T_{\rm eff}$–colour relations of (Boyajian et al. 2012). We assumed a Pleiades metallicity [Fe/H] $=0.02\pm0.03$ (Funayama et al. 2009; Soderblom et al. 2009). Assuming a typical Pleiades extinction of $A_V=0.12$ and using reddening coefficients from Yuan et al. (2013), we estimated $T_{\rm eff}$ of 4670 ± 250 and 4910 ± 100 from $B-V$ and $V-K$, respectively. The convolved probability distribution has a mean of 4870 ± 90 K. If extinction is negligible, the mean is 4790 ± 90 K. If the star is actually metal-rich, the derived $T_{\rm eff}$ is hotter, but only by 20–30 K.

We made an independent estimate of $T_{\rm eff}$ based on comparing our combined visible-wavelength (SNIFS) and near-infrared (SpeX) spectra with stellar models (Section 2.2). The combined spectrum was compared to the Göttingen spectral library constructed using the PHOENIX model in spherical mode (Husser et al. 2013). The spectrum was re-sampled at higher resolution and uniformly with logarithmic wavelength. Medium-resolution ($R=10\,000$) model spectra were convolved with a Gaussian to the approximate resolution of the observed spectrum and re-sampled at the same wavelengths. Model wavelengths were converted from vacuum to air using the formula of Morton (1991) and the maximum of the cross-correlation function with the observed spectrum used as a pseudo-Doppler shift. The shifted spectrum was then used to compute χ^2 for each possible model. Multiple regions of the spectrum that were previously identified as problematic or contaminated by telluric lines were excluded (Gaidos et al. 2014). The 25 best-fitting models were then used to construct 10 000 linear interpolations to compare with the model via χ^2.

The best-fitting interpolated model with no correction for reddening has $T_{\rm eff}=4770$ K, $\log g=3.72$, and [M/H] $=+0.5$ ($\chi^2_\nu=1.24$). When the spectrum was dereddened ($E_{B-V}=0.04$), the best-fitting model has $T_{\rm eff}=4870$ K, $\log g=3.4$, and [M/H] $=-0.5$. The temperatures are within one standard deviation of the values derived from photometry. On the other hand, $\log g$ and [M/H] cannot be reliably estimated from K dwarf spectra with this resolution and we consider these 'nuisance' parameters to be ignored. We calculated 95 per cent confidence intervals of 90 K for $T_{\rm eff}$ based on the distribution of χ^2 values.

Parameter values were also derived by comparing, order by order, the high-resolution spectrum obtained with *Subaru*/HDS with the version 2.0 Göttingen library of PHOENIX model spectra (Husser et al. 2013). The resolution of the grid was 100K in $T_{\rm eff}$, 0.5 dex in [Fe/H], and 0.5 in $\log g$. Spectra were interpolated on to a logarithmic wavelength grid to facilitate Doppler shifting, and normalized and de-trending by a cubic spline fit. Model spectra wavelengths were converted to values in air using the relation of Morton (1991), the spectra were convolved with a series of Gaussians of different widths to account for rotational broadening, cross-correlated and shifted with respect to the observed spectra, and the results compared to the observations by a χ^2 calculation, after removal of any second-order trend, with Doppler shift and broadening as the two free parameters. The best-fitting model has $T_{\rm eff}=4900$ K, [Fe/H] $=0$, and $\log g=5.0$, consistent with our results using photometry and low-resolution spectra. The best-fitting broadening is 6.6 km s^{-1}, equal to the instrument resolution. Thus, any rotational broadening is less than a few km s^{-1}, further evidence that the star is a slow rotator (Section 3.3).

Finally, a line-by-line (Fe I and Fe II) analysis of the HDS spectrum was performed using the methods described in Takeda, Ohkubo & Sadakane (2002) and Hirano et al. (2014). The derived parameters are similar: $T_{\rm eff}=4970\pm45$ K, [Fe/H] $=0.29\pm0.06$, $\log g=4.47\pm0.13$, and $v\sin i=4.0$ km s^{-1} (for a microturbulence parameter of $\xi=1.5$ km s^{-1}). These values are more precise, and consistent with the other values, and we adopt them for the stellar parameters (Table 2). The bolometric flux was determined by integrating over the flux-calibrated spectrum: $f_{\rm bol}=5.06\pm0.16\times10^{-13}$ W m^{-2}. Adopting the spectroscopic value for $T_{\rm eff}$ (4970 K) and the kinematic distance 125 ± 5 pc, we estimated the radius to be $R_*=0.67\pm0.03\,{\rm R}_\odot$. Employing the empirical relation with $T_{\rm eff}$ constructed by Boyajian et al. (2012) and considering all errors, including the intrinsic scatter in the relation itself, we found $R_*=0.76\pm0.03\,{\rm R}_\odot$. The (photometric) distance at which the two radius estimates are in agreement is 141 ± 6 pc, identical to within error of the VLBI-based Pleiades distance. The stellar luminosity is then $M_K=4.05\pm0.10$ and its mass, based on the empirical relation developed by Henry & McCarthy (1993), is $0.78\pm0.12\,{\rm M}_\odot$. The bolometric luminosity, uncorrected for any extinction, is $0.316\pm0.026\,{\rm L}_\odot$. The resulting stellar $\log g$ is 4.58 ± 0.07, within 1σ of the spectroscopic value.

4 ANALYSIS: THE PLANET

4.1 Light-curve fitting

We fit the *K2* light curve with a Monte Carlo Markov Chain (MCMC) as described in Mann et al. (2016b), which we briefly summarize here. We used the EMCEE PYTHON module (Foreman-Mackey et al. 2013) to fit the model light curves produced by the tbatman package (Kreidberg 2015) using the Mandel & Agol (2002) algorithm. Following Kipping (2010), we oversampled and binned the model to match the 30 min cadence. We sampled the planet-to-star radius ratio ($R_{\rm P}/R_*$), impact parameter (b), orbital period (P), epoch of the first transit mid-point (T_0), mean stellar density ρ_*, and two limb-darkening parameters (q_1 and q_2), and two parameters that describe the orbital eccentricity (e) and argument of periastron (ω): $\sqrt{e}\sin\omega$ and $\sqrt{e}\cos\omega$. We assumed a quadratic limb-darkening law and used the triangular method of Kipping (2013) to sample the

Table 1. Transit fit parameters.

Parameter	Fit 1[a]	Fit 2[a]
Period (d)	$8.199\,833^{+0.000\,681}_{-0.000\,691}$	$8.199\,796^{+0.000\,683}_{-0.000\,719}$
R_P/R_*	$0.0273^{+0.0016}_{-0.0008}$	$0.0278^{+0.0022}_{-0.0011}$
T_0 (BJD-2400000)	$57070.80576^{+0.001\,74}_{-0.001\,74}$	$57070.80596^{+0.00190}_{-0.00179}$
Impact parameter	$0.32^{+0.29}_{-0.22}$	$0.46^{+0.24}_{-0.30}$
Density (Solar)	$2.5^{+0.5}_{-1.0}$	$1.8^{+0.3}_{-0.3}$
Duration (h)	$2.62^{+0.08}_{-0.08}$	$2.40^{+0.35}_{-0.75}$
Inclination (°)	$89.2^{+0.5}_{-1.0}$	$88.7^{+0.8}_{-0.8}$
a/R$_*$	$23.3^{+1.4}_{-3.6}$	$23.2^{+6.4}_{-2.3}$
Eccentricity	0 (fixed)	$0.14^{+0.22}_{-0.09}$
ω (°)	0 (fixed)	1^{+106}_{-114}
u1[c]	$0.70^{+0.08}_{-0.08}$	$0.60^{+0.08}_{-0.08}$
u2[c]	$0.13^{+0.07}_{-0.07}$	$0.12^{+0.07}_{-0.07}$

[a]Fit 1 is done with e and ω fixed to 0 and a uniform prior on ρ_*. Fit 2 is done with a Guassian prior on ρ_* from Section 4 but no constraints on $\sqrt{e}\sin\omega$ and $\sqrt{e}\cos\omega$.
[b]BJD is reported as Barycentric Dynamical Time.
[c]Linear and quadratic limb-darkening coefficients.

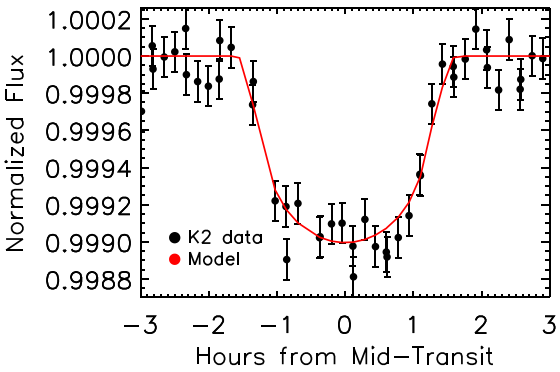

Figure 8. Phase-folded light curve of EPIC 210363145 (black) from *K2*. The best-fitting (highest likelihood) transit model is shown in red.

2D parameter space. We applied a prior on limb darkening derived from the Husser et al. (2013) atmospheric models, calculated using the LDTK toolkit (Parviainen & Aigrain 2015).

We ran two separate MCMC analyses, the first ('Fit 1') with $\sqrt{e}\sin\omega$ and $\sqrt{e}\cos\omega$ fixed at zero and ρ_* under a uniform prior, and the second ('Fit 2') with both $\sqrt{e}\sin\omega$ and $\sqrt{e}\cos\omega$ allowed to explore [0,1) under uniform priors, but with a Gaussian prior on ρ_* derived from our stellar parameters in Section 3.5. All other parameters were explored with only physical limitations (e.g. $P > 0$) and uniform priors. MCMC chains were run using 200 walkers, each with 100 000 steps after a burn-in phase of 10 000 steps (determined from trial and error on known systems).

We report the transit fit parameters in Table 1. For each parameter, we report the median value with the errors as the 84.1 and 15.9 percentile values (corresponding to 1σ for Gaussian distributions). The model light curve with the best-fitting parameters is shown in Fig. 8. We also show posteriors and correlations for a subset of parameters in Fig. 9.

The stellar density derived from Fit 1 is consistent with the spectroscopy-based stellar density derived in Section 4, as we show in Fig. 10. This is consistent with our second transit fit, which suggests a small or even zero eccentricity, and yields a density consistent with the spectroscopic/distance-based estimate.

4.2 False positive probability

We calculated the false positive probability (FPP) that the transit signal could be produced by an unresolved background eclipsing binary or transiting planet system using the Bayesian procedure described in Gaidos, Mann & Ansdell (2016b). This calculation uses as a prior the TRILEGAL model (v. 1.6) of the background Galactic stellar population at the location of EPIC 210363145, and imposes constraints from transit depth, the duration of the transit, and the lack of additional sources in NIRC2-AO and NRM imaging. No constraint on image centroid shift is imposed due to the much greater image jitter of the *K2* mission. The calculation does not consider the probability that a background star actually is an eclipsing binary or transiting system, only that it could produce the observed transit properties given the observation constraints, and thus is conservative. The resulting FPP after 100 iterations of 10 000 Monte Carlo simulations each is 7.5×10^{-7}.

Alternatively, the transit signal could be produced by an unresolved companion to EPIC 210363145 that is an eclipsing binary or transiting planetary system. We limited this set of scenarios by considering the posterior distribution of the density of the host star produced by the transit fit (Fig. 10). The limit of $\rho_* < 3.8\rho_\odot$ limits the contrast ratio between EPIC 210363145 and a possible companion star, and thus limits the radius of the tertiary that could produce the transit. To calculate these limits, we used the empirical, model-independent masses and radii of nearby late K and M dwarfs established by Mann et al. (2015) and the apparent *Kepler* magnitudes determined in Gaidos et al. (2016a), along with the additional constraint that the metallicity of the secondary must be within 2σ of the primary ($0.17 < [\mathrm{Fe/H}] < 0.41$). We found that any companion responsible for the transit signal can be no cooler than early M-type ($T_{\rm eff} > 3600$ K), that the *Kepler* $K_{\rm p}$ contrast must be <3 mag. The transiting object would be at most 3 per cent larger (the case of maximum contrast ratio and minimum dilution) and still* $<6R_\oplus$, i.e. a planet and not an eclipsing binary. The contrast ratio in the K'-band of NIRC2 must be <1.5 mag and since no such companion was detected in our NRM imaging, if it exists it must be within 0.02 arcsec or ∼3 au of the primary (Fig. 3). The reflex motion of the primary induced by such a companion would be at least several km s^{-1}, but could have remained unresolved due to the short timespan (one month) of our RV observations (Section 2.3). Additional observations will readily detect or rule out any such companion.

4.3 RVs and planet mass

The three RV measurements from IGRINS are plotted versus orbital phase (0 = transit centre) and with their relative error bars in Fig. 11. Assuming that RV variation is due exclusively to the presence of the transiting planet, as well as a circular, edge-on orbit, we placed an upper limit on the planet mass. For each possible mass (and corresponding Doppler RV amplitude), we fit for the only remaining free parameter – the system barycenter velocity – and calculated χ^2. We identified the mass for minimum χ^2 (0.3 Jupiter masses M_J, $\chi^2 = 6.4$, $\nu = 2$) but also a much more meaningful 99 per cent upper limit of $1.9M_J$ based on χ^2 ($\Delta\chi^2 < 5.0$). This rules out a stellar or brown dwarf mass for the transiting object. Although we have neglected astrophysical noise (stellar 'jitter') in our analysis, this is expected to be comparatively small at infrared wavelengths

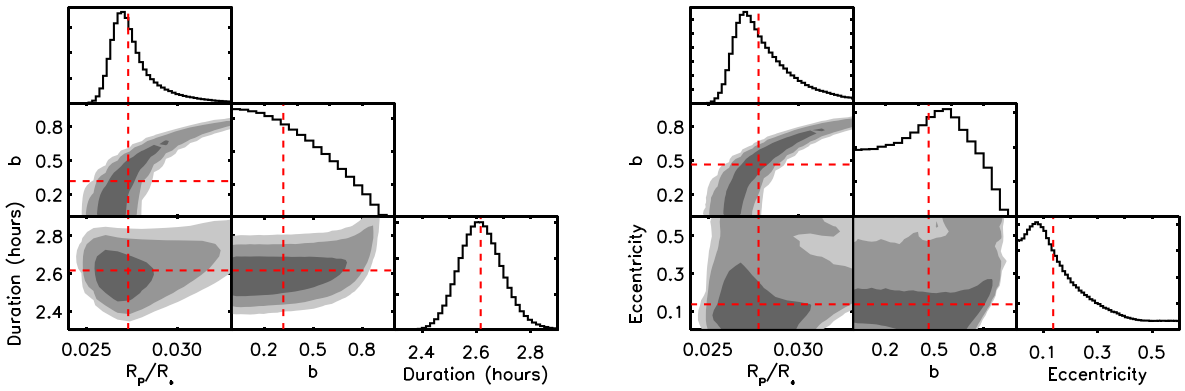

Figure 9. Posteriors (histograms) and parameter correlations (contour plots) from our MCMC fits to the *K2* light curves. Median values for each parameter are marked with red dashed lines. Grey shading covers 67 per cent, 95 per cent and 99 per cent, from dark to light, of the MCMC posterior. The left plot shows the posteriors when e is set to zero (Fit 1), while the right is from the fit where these are allowed to float but with a density prior (Fit 2).

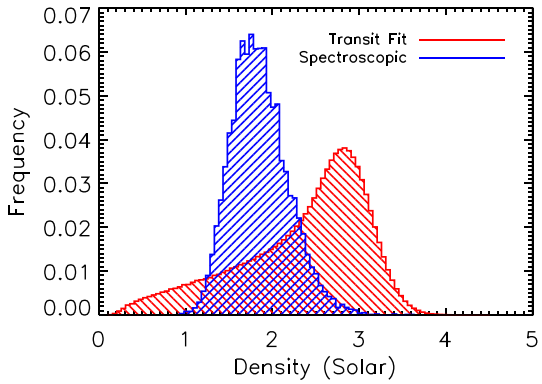

Figure 10. Stellar density posterior from the transit fit (red) and from our stellar parameters derived independently from spectroscopy in Section 3.5 (blue). The transit fit assumes $e = 0$.

(Marchwinski et al. 2015) and much less than the typical measurement error of $\sim$100 m s^{-1}.

5 DISCUSSION

5.1 The nature of EPIC 210363145 and its planet

Our estimates of the properties of the EPIC 210363145 system are summarized in Table 2. EPIC 210363145 was identified as a Pleiades member with high confidence based on its proper motion and photometric distance, but our detailed analysis of the star's properties contradict this. It does not appear in the Pleiades member catalogues of Stauffer et al. (2007) or Sarro et al. (2014). The star is located at approximately the same distance as the cluster, but it is at $\approx$28 pc, about twice the tidal radius, from the cluster centre. Assuming the photometric distance is correct, the space motion of EPIC 210363145 is actually distinct from that of the Pleiades by 5.4 ± 0.9 km s^{-1}, or about nine times the cluster's velocity dispersion. The star's relative motion is currently at a right angle ($92 \pm 12^\circ$) to the vector between the star and the Pleiades, inconsistent with EPIC 210363145 as a 'runaway' from the cluster. A differential vertical velocity of 8–9 km s^{-1} imposed by the Galactic potential would bring the original angle to $8 \pm 5^\circ$, but this is unlikely to have occurred in a single vertical oscillation lasting a few tens of Myr. Although the star is rotationally variable and a NUV source, its rotation period is 20 d, twice as long as the most slowly rotating

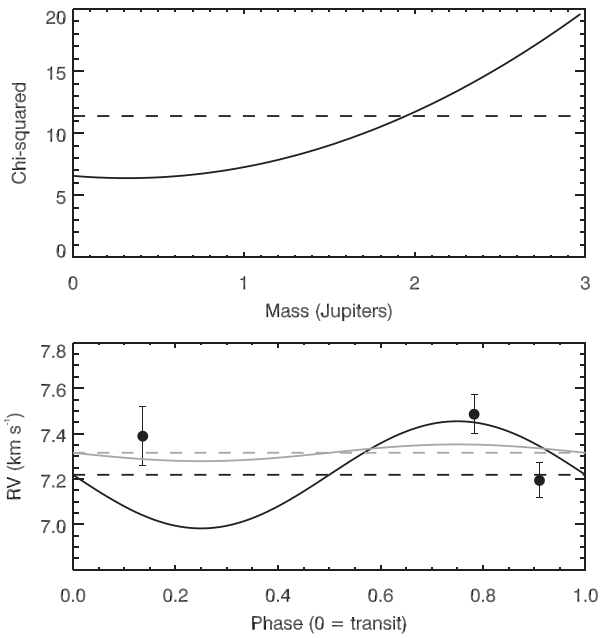

Figure 11. Top: χ^2 of fits of a Keplerian circular, edge-on orbit with a period and phase set by the transit ephemeris to the RV data of EPIC 210363145 obtained with the IGRINS spectrograph. The single free parameter is the radial velocity of the system barycenter. The dashed line shows the limit on χ^2 corresponding to the 99 per cent confidence interval. Bottom: Barycentric radial velocities phased to the orbit along with the best-fitting model (solid grey) and its barycenter value (dashed grey) and 99 per cent upper limit model (black solid) and its barycenter value (dashed black).

Pleiades stars, and its spectrum lacks Hα emission. Finally, it is significantly more metal-rich (by $\approx$0.26 dex) than the typical Pleiades member.

The star does not appear kinematically related to any other known cluster or nearby young moving group. The AB Doradus moving group may be related to the Pleiades via a similar age (Luhman et al. 2005) and kinematics (Ortega et al. 2007), but its known members are much closer than EPIC 210363145. Nevertheless, EPIC 210363145 is moving comparatively slowly ($\Delta v \approx 16$ km s^{-1} and $\Delta UVW = +3.1, -15.3, -3.0$ km s^{-1}) with respect to the Local Standard of Rest (LSR) as defined by Coşkunoğlu et al. (2011) and is probably young. According to the age–kinematic relations of Nordström et al. (2004), such motion is characteristic of

Table 2. Properties of the EPIC 210363145 system.

Parameter	Value
Observed:	
RA (J2000)	$03^{h}40^{m}54^{s}.82$
Dec.	$12^{\circ}\,34'\,21''.4$
μ_{RA}	$+23.5 \pm 1.3$ mas yr^{-1}
μ_{δ}	-37.9 ± 1.7 mas yr^{-1}
(U, V, W)	$(-5.4 \pm 0.6, -28.7 \pm 1.0, -9.5 \pm 0.9)$ km s^{-1}
B	13.229 ± 0.030
V	12.158 ± 0.093
g	12.717 ± 0.019
r	11.813 ± 0.087
i	11.531 ± 0.060
J	10.384 ± 0.020
H	9.910 ± 0.023
K_s	9.799 ± 0.018
Inferred (star):	
Dist. (kinematic)	125 ± 7 pc
Dist. (photometric)	141 ± 6 pc
RV	7.35 ± 0.20 km s^{-1}
$T_{\rm eff}$	4970 ± 45 K
Fe/H	$+0.29 \pm 0.06$ dex
log g	4.47 ± 0.13
R_*	0.76 ± 0.03 R$_\odot$
M_*	0.80 ± 0.12 M$_\odot$
L_*	0.316 ± 0.026 L$_\odot$
$P_{\rm rot}$	19.8 ± 2.9 d
$v \sin i$	4.0 km s^{-1}
Age (gyrochronology)	0.4-1.3 Gyr
Inferred (planet):	
Planet radius	2.30 ± 0.16 R$_\oplus$
Planet mass	$<1.9 M_J$
Orbital period	8.1998 ± 0.0007 d
Orbital inclination	$88.7 \pm 0.8^{\circ}$
Orbital eccentricity	$0.14^{+0.22}_{-0.09}$
Stellar irradiance	58 ± 7I$_\oplus$

an age of <1 Gyr. (The median accuracy of that relation is given as 25 per cent.) Curiously, most of the motion with respect to the LSR is in the direction of Galactic rotation (V) and not U, but this cannot be due to differential Galactic rotation alone over reasonable scales, i.e. if the Oort constants $A + B$ are $\sim$2.5 km s^{-1}kpc^{-1} (Feast & Whitelock 1997).

The star's 20-d rotation period places it between the 450 Myr and 1 Gyr gyrochrones of Barnes (2007), indicating a young but not Pleiades-like age. The revised gyrochronology of Mamajek & Hillenbrand (2008) predicts an age of 1.3 Gyr with an error of 0.34 Gyr from the uncertainty in the rotation period, and 0.16 Gyr from the scatter about the best fit. The high metallicity and slow rotation nicely explain the absence of lithium in EPIC 210363145. Lithium depletion is vastly accelerated in metal-rich pre-main-sequence stars because the higher opacity deepens the base of the convective zone, mixing Li to higher temperatures where it is destroyed. The predicted effect for zero-age main sequence (ZAMS) stars is $\geq$1 dex decrease in Li for each 0.1 dex increase in [Fe/H] (Somers & Pinsonneault 2014), and Li in EPIC 210363145 would have been depleted to undetectable levels by a Pleiades-like age. Lithium abundance also correlates with rotation (e.g. Soderblom et al. 1993; Chaboyer, Demarque & Pinsonneault 1995), and the relationship appears to depend on stellar mass and switch sign at $M_* \approx 1$ M$_\odot$, becoming positive (and stronger) for stars with $T_{\rm eff}$ < 5500 K. Somers & Pinsonneault (2015) proposed that in cooler stars, pre-main-sequence destruction of Li is extremely sensitive to the central temperature and hence interior structure of the star, and is inhibited by inflation of the stellar radius. If radius inflation is related to magnetic fields (Feiden & Chaboyer 2013), which are, in turn, related to stellar rotation, then more rapidly rotating, magnetically active stars will have more lithium, as is observed. Conversely, a slow rotator such as EPIC 210363145 will be magnetically inactive, have experienced no inflation, and have suffered the full lithium depletion predicted for such objects (Somers & Pinsonneault 2015).

EPIC 210363145 emits detectable flux at NUV wavelengths consistent with a Pleiades age but no Hα. The reliability of the NUV detection by *GALEX* ($m \approx 20$) is about 99 per cent.[3] The de-reddened $m_{\rm NUV} - J$ colour of EPIC 210363145 is 8.8 and about 1.9 mag 'bluer' (NUV brighter) than an extrapolation of the locus of inactive field stars described by Ansdell et al. (2015). An M dwarf star with such a $m_{\rm NUV} - J$ colour typically has Hα emission with an EW of $\sim$4 Å (note that EPIC 210363145 is an early K dwarf). However, the expected Hα emission may be smaller considering that, since EPIC 210363145 does not appear to be a Pleiades member and does not lie along the line of sight to the cluster centre, the extinction may be negligible. In this case, the star's $m_{\rm NUV} - J$ is redder ($\approx$9.6) and only 1.1 mag 'bluer' than the locus of inactive stars. The expected EW of Hα emission is $\sim$2 Å, however the scatter spans values from zero to twice this value. This scatter could be the result of multiyear-long cycles of stellar activity. For example, observations in 1988 by Soderblom et al. (1993) identified several bona fide Pleiades members lacking significant Hα emission, including Trumpler HII3179 (HD 24194). Observations by White, Gabor & Hillenbrand (2007) 14 yr later found HD 24194 to have Hα emission with an EW of 3.16 Å(HD 24194). Likewise, the absence of Hα emission from EPIC 210363145 may be due to the 8+ yr between the epochs of the *GALEX* (pre-2008) and SNIFS observations.

We ruled out two alternative explanations for the absence of Hα emission: *GALEX* confusion with an unrelated background source, or a white dwarf companion which has UV flux but no Hα emission. We calculated the probability of source confusion by identifying all *GALEX* DR5 AIS+MIS sources with $m_{\rm NUV} < 20$ within 10 arcmin of the position of EPIC 210363145 and multiplying this count by the ratio of the solid angle of the *GALEX* point response function, conservatively approximated as a circle of radius 7 arcsec (Morrissey et al. 2007), to the query area. The result is a confusion probability of 1×10^{-3}. Even if we include all detected sources regardless of NUV magnitude, the probability only rises to 2 per cent. A white dwarf companion is ruled out by our RV data (Sec. 4.3).

To coherently constrain the properties of EPIC 210363145, we performed a global parameter inference by comparing our observations to a grid of stellar evolution models. Model calculations were performed with an updated version of the Dartmouth stellar evolution code (Dotter et al. 2008; Feiden & Chaboyer 2013) in which a number of improvements were made to more accurately model the properties of pre-main-sequence stars (Feiden 2016). The grid of non-magnetic models covered a mass range of 0.1–0.9 M$_\odot$ with a resolution of 0.02 M$_\odot$ and a metallicity range of $-$0.5 to +0.5 dex at a resolution of 0.1 dex. The MCMC method implemented as EMCEE (Foreman-Mackey et al. 2013) was used to explore possible values of stellar mass, metallicity [M/H], age, and distance and find the combination that most closely reproduces the stellar $T_{\rm eff}$, bolometric flux $F_{\rm bol}$, and mean density ρ_* using the likelihood function described in Mann et al. (2015). We applied Gaussian priors on distance (130 ± 20 pc) and metallicity ($+0.3 \pm 0.1$ dec) and

[3] http://www.galex.caltech.edu/researcher/techdocs.html

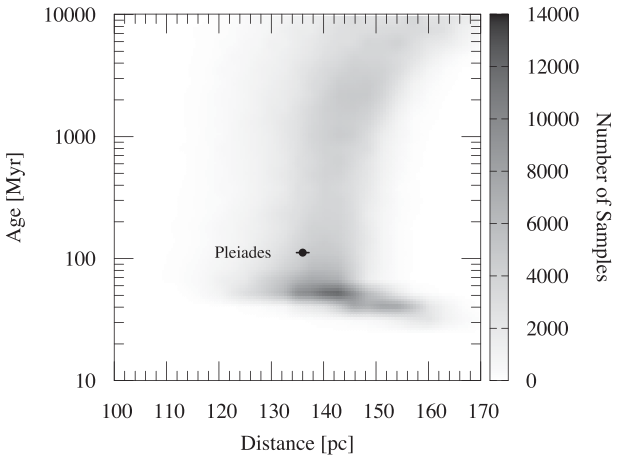

Figure 12. Joint posterior distribution of estimated age and distance of EPIC 210363145, calculated by MCMC inference of stellar parameters performed by comparing $T_{\rm eff}$, [Fe/H], and bolometric flux to the predictions of a stellar evolution model. The location of the Pleiades (112 ± 5 Myr, 136 ± 1.2 pc) is marked.

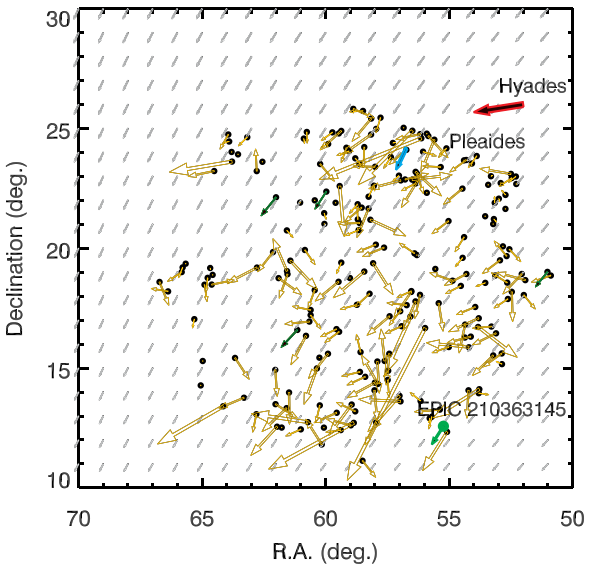

Figure 13. Locations of 218 candidate K dwarfs observed by *K2* in the C4 field which exhibit a periodic signal (e.g. from rotational variability) in their light curve but which were not identified as members of the Pleiades or Hyades clusters. The gold arrows indicate the direction and magnitude of proper motion (PM), if any. The location and PM of EPIC 210363145 and the Pleiades centre are shown by the green and blue arrows, respectively. The other thin green arrows are variable K dwarf stars which have PMs within 20 per cent of EPIC 210363145. The Hyades PM (but not location) is indicated by the red arrow. The grid of grey arrows indicates the PM of a star in the Local Standard of Rest, i.e. the PM is due only to the Sun's motion.

uniform priors to mass (0.1–0.9 $M_\odot$) and logarithmic age (0.1 Myr–14 Gyr). (We ran a second set of simulations with a tighter distance prior, and found nearly identical results.) The MCMC calculation was performed with 300 walkers initially assigned to random positions in parameter space. An initial 'burn-in' sequence of 2000 iterations was used to seed a second sequence of 3000 iterations and then discarded. The second sequence was used to calculate the posterior probability distributions for the stellar parameters (chains were not thinned). Convergence was evaluated by visually inspecting trace plots for all 300 chains to identify any systematic trends or noticeably poor mixing. In addition, we verified that the median acceptance fraction among the ensemble of chains was 25–50 per cent and the length of each chain was at least five times the autocorrelation length. We computed the Gelman–Rubin scale reduction factor R (Gelman & Rubin 1992) for each of the fitted parameters. All of the fitted parameters have $1.1 < R < 1.2$ and the values of R are flat along the final 1000 iterations, indicating that the chains are well mixed and convergence has been obtained.

Our model comparison found the most probable properties for EPIC 210363145 to be $M_* \geq 0.89\,M_\odot$, $R_* = 0.78\,R_\odot$, [M/H] = +0.26 dex, a distance of 143 pc, and an age of 50 Myr, although a wide range of older ages consistent with gyrochronometry is allowed. We do not report formal uncertainties with these values as they are highly correlated and the preferred mass is at the edge of the model grid. The model-based values are broadly consistent with the spectroscopically and empirically determined values, in part due to the priors. Demonstrating further consistency, the 95 per cent confidence range for log g is 4.49–4.65, compared to the spectroscopic value of 4.47 ± 0.13. The models assign the star a higher mass and slightly greater radius and distance, but this can be explained by the effect of high metallicity. At a given $T_{\rm eff}$, R_* increases with [M/H], requiring a larger distance to reproduce $F_{\rm bol}$. For a given M_*, higher [M/H] causes a decrease in $T_{\rm eff}$, thus, higher metallicity increases the required M_* to reproduce the observed $T_{\rm eff}$. However, the effect of metallicity was not included in the empirical relations of Boyajian et al. (2012) and Henry & McCarthy (1993) due to insufficient numbers of calibrator stars. A larger stellar radius would mean that the planet is also proportionally larger.

Fig. 12 shows the joint posterior distribution of age and distance, marking the Pleiades mean distance and age. Posterior distances are slightly, but not significantly farther than the centre of the Pleiades and at a given distance, there is a large range of possible ages. Most curious is the preferred age of 50 Myr, the main-sequence 'age zero' (ZAMS) of a star with 0.9 $M_\odot$ and [M/H] = +0.3, although older ages are not excluded. For a given $T_{\rm eff}$ and [Fe/H], the ZAMS is a minimum in luminosity and maximum in mean density. Luminosity can be traded against distance when bolometric flux is fixed, and the best-fitting distance is not extreme. On the other hand, it appears that the transit-based stellar density constraint, which is skewed towards higher values than the empirical/spectroscopy-based value (Fig. 10), drives many MCMC solutions to the ZAMS. The choice of a uniform prior with logarithmic age could also bias solutions towards erroneously young ages. We performed a second set of simulations with a uniform prior with linear age, appropriate for the case of a constant star formation rate (SFR). Note that a higher early SFR would shift the best prior towards older ages, but the location of the C4 field near the Galactic mid-plane would shift the prior towards younger ages. The posteriors from this second run rule out ages <50 Myr and an age of ∼150 Myr is (slightly) preferred, although older ages are possible.

Is EPIC 210363145 a loner, or instead only one of a population of variable dwarf stars with similar kinematics? We identified 973 stars observed by *K2* in the C4 field that are candidate field K dwarfs, i.e. have estimated $T_{\rm eff}$ in Huber et al. (2016) between 4200 and 5200 K and log $g > 4.1$, but are not identified as members of the Hyades or Pleiades clusters by Mann et al. (2016b) or this work. We analysed the *K2* light curves of these stars using the ACF-based method described in Section 3.3. A periodic signal was identified in 218 of these stars. Fig. 13 plots their locations and proper motions as well as those of EPIC 210363145 and the Pleiades and Hyades clusters. There are many rotationally variable stars

with proper motions in roughly the same (southeast) direction as EPIC 210363145. The star with the largest proper motion is BD+16 502/GJ 9122A, an active K7 dwarf only 18 pc away (Reid & Cruz 2002). This phenomenon is merely the result of the Sun's motion with respect to the LSR. We calculated the this apparent motion using the LSR of Coşkunoğlu et al. (2011) and the photometric distance of EPIC 210363145 and this is plotted as the grid of grey arrows in Fig. 13. To identify potential kinematic relatives of EPIC 210363145, we iteratively selected those variable K dwarfs that have PMs within 5σ of their mean, using the proper motion of EPIC 210363145 as the initial value. We identified four such stars besides EPIC 210363145, plotted as green arrows in Fig. 13. All were rejected as Pleiades members, they have a wide range of rotation rates and photometric distances, and their similar proper motions appears to be coincident.

Overall, the properties of EPIC 210363145 indicate that it is unrelated to and probably older than the Pleiades, but younger ($\lesssim$1.3 Gyr) than most field stars. If so, its proximity to the Pleiades in dynamical phase space is a coincidence, and a warning that membership probability calculations based only on space motion and photometric distance are not immune from interlopers. On the other hand, it is possible that this star tells us that very slow rotation is no disqualifier for a young age: Stauffer et al. (2016) reported four F dwarf and seven M dwarf Pleiades members with anomalously low rotation rates; they attribute the phenomenon among F dwarfs to binarity, but for the M dwarfs, all of which have $P > 10$ d and some of which exhibit weak Hα emission, they offer no explanation. A precise parallax and proper motion from the *Gaia* astrometric mission will allow us to further refine the properties of this enigmatic star and its planet.

The planet's maximum plausible mass, assuming an Earth-like rock-metal composition, is $\sim 50 M_\oplus$ (Swift et al. 2012) and the commensurate Doppler signal would be $\sim$20 m s^{-1}, well below our current RV limit. However, the planet radius falls in a regime where many combinations of mass–radius measurements suggest planets have thick hydrogen–helium envelopes (Rogers 2015). In that case, adopting the nominal mass–radius relation of Weiss & Marcy (2014), the planet mass is predicted to have $\sim 6 M_\oplus$ and the Doppler signal is only 2 m s^{-1}. This would be possible to detect using sufficiently sensitive instruments such as ESPRESSO on the VLT (Pepe et al. 2014), provided photospheric 'jitter' from spots does not overwhelm the signal.

5.2 Occurrence of Pleiades planets

Our analysis of the *K2* light curves of about 1000 candidate Pleiades members has thus far revealed only this single planet around a host star of questionable membership. This begs the question: where are the Pleiades planets? *Kepler* discovered several thousand candidate planets around $\sim$200 000 stars, a rate of $\sim$2 per cent, but of course, *K2* observed the Pleiades for a much shorter interval of time, the photometric noise due to pointing error is larger, and Pleiades stars are more active and rotationally variable. To address the question of whether the absence of Pleiades detections reflects a difference in planet population or is the result of lower detection efficiency, we performed numerical injection-and-recovery experiments on the *K2* light curves assuming the null hypothesis, i.e. the same population of planets around *Kepler* stars also orbits around the Pleiades.

The transit signal from a single simulated planet on a circular orbit was injected into each of 10 replicate light curves of the 1014 Pleiades candidates with values for $T_{\rm eff}$, radius, and mass in the EPIC catalogue. Planet radii were randomly selected from the intrinsic distribution calculated by Silburt, Gaidos & Wu (2015) for FGK dwarfs ($T_{\rm eff} > 3900$ K) and from Gaidos et al. (2016b) for cooler M dwarfs. Orbital periods were selected from a logarithmic uniform distribution over 3–25 d. Transits were simulated with a random phase, an impact parameter selected from a uniform distribution and a quadratic limb-darkening law with coefficients selected from Claret & Bloemen (2011) for the EPIC values of $T_{\rm eff}$. Transits were recovered (or not) using the light curve processing and BLS search routine described in Section 2.1. A planet was deemed 'recovered' if the orbital period P fell within 2.5σ of the true value, where $\sigma = P/N_{\rm ind}$, and $N_{\rm ind}$ is the number of independent frequencies. (σ is the effective spectral resolution of the BLS search.) Inspection of the distribution of deviations of recovered from 'true' orbital periods showed that this criterion sufficed to capture essentially all detections.

The geometric probability of a circular transiting orbit was calculated and summed for all detections. This sum represents the expected number of detections if every star has one planet with the properties in the specified ranges. To make an actual estimate, this was multiplied by the estimated occurrence based on published *Kepler* statistics. For this step, we divided systems into FGK and M dwarfs as occurrence seems to differ markedly between spectral types (Mulders et al. 2015; Gaidos et al. 2016b). Estimates of the occurrence of planets around solar-type stars vary: Howard et al. (2012) found 0.24 per star for planets >1 R$_\oplus$ on 3.4–29 d orbits; Petigura, Howard & Marcy (2013) found 0.23, which when corrected for planets <1 R$_\oplus$ using the radius distribution of close-in planets is 0.28. Silburt et al. (2015) found about 0.25 for planets 1–4 R$_\oplus$, which when corrected for smaller and larger planets is about 0.33, a value we used here. The occurrence of planets close to M dwarfs is significantly higher: Gaidos et al. (2016b) estimated that M dwarfs host 2.2 ± 0.3 1–4 R$_\oplus$ planets with $P < 180$ d, consistent with previous estimates (Morton & Swift 2014; Dressing & Charbonneau 2015). The occurrence for $P < 25$ d is 1.45.

The predicted number of detection is 0.39 among the 411 FGK Pleiades dwarfs and 0.44 among the 603 M dwarfs, for a total of $\sim$0.83 detections. A separate analysis of the same set of synthetic light curves with a modified version of the K2SSF pipeline (Mann et al. 2016a; Vanderburg et al. 2016) predicted 1.27 detections among FGK dwarfs and 0.51 among the M dwarfs, for a total yield of 1.78. The Poisson probabilities of having no detections are thus 0.44 and 0.17, respectively. Thus, the null hypothesis of a *Kepler* -like planet population cannot be ruled out, and the absence of detections among Pleiades stars is at least, in part, the product of the steep distribution of planet occurrence with radius and the difficulty of detecting small planets around young, photometrically variable stars with *K2* data, at least with our current analysis tools. In particular, transit signals with orbital periods corresponding to a period (or harmonic) of the stellar variability may be attenuated in the filtering step. Another possible factor is if the radii of Pleiades stars were systematically underestimated in the EPIC catalogue, e.g. because the effect of reddening, which makes stars appear cooler and therefore smaller, or because some Pleiades M dwarfs may not have entirely evolved to the main sequence. The former effect is small: for EPIC 210363145, the difference in the photometric colour-based radii is $\sim$2 per cent for $E_{B-V} = 0.04$ versus $E_{B-V} = 0$. The upcoming *TESS* mission (Ricker et al. 2014), which will survey the sky at a comparable sensitivity and with a similar time baseline, may offer only limited improvement in the situation. Data from the PLATO mission (Rauer et al. 2014) are more likely to yield advances, provided the appropriate fields are observed.

ACKNOWLEDGEMENTS

This research was supported by NASA Origins of Solar Systems grant NNX11AC33G to EG, NSF grants AST-1518332 to RJDR, JRG, and TME, and NASA grants NNX15AD95G/NEXSS and NNX15AC89G to RJDR, JRG, and TME. ALK acknowledges support from a NASA Keck PI Data Award administered by the NASA Exoplanet Science Institute, and from NASA XRP grant 14-XRP14 2-0106. NN acknowledges supports by Grant-in-Aid for Scientific Research (A) (JSPS KAKENHI Grant Number 25247026). SNIFS on the UH 2.2-m telescope is part of the Nearby Supernova Factory project, a scientific collaboration among the Centre de Recherche Astronomique de Lyon, Institut de Physique Nucleaire de Lyon, Laboratoire de Physique Nuclaire et des Hautes Energies, Lawrence Berkeley National Laboratory, Yale University, University of Bonn, Max Planck Institute for Astrophysics, Tsinghua Center for Astrophysics, and the Centre de Physique des Particules de Marseille. Based on data from the Infrared Telescope Facility, which is operated by the University of Hawaii under Cooperative Agreement no. NNX-08AE38A with the National Aeronautics and Space Administration, Science Mission Directorate, Planetary Astronomy Program. This work used the Immersion Grating Infrared Spectrometer (IGRINS) that was developed under a collaboration between the University of Texas at Austin and the Korea Astronomy and Space Science Institute (KASI) with the financial support of the US National Science Foundation under grant AST-1229522, of the University of Texas at Austin, and of the Korean GMT Project of KASI. Some/all of the data presented in this paper were obtained from the MAST. STScI is operated by the Association of Universities for Research in Astronomy, Inc., under NASA contract NAS5-26555. Support for MAST for non-*HST* data is provided by the NASA Office of Space Science via grant NNX09AF08G and by other grants and contracts. This research has made use of the NASA/IPAC Infrared Science Archive, which is operated by the Jet Propulsion Laboratory, California Institute of Technology, under contract with the National Aeronautics and Space Administration. This research made use of the SIMBAD and VIZIER Astronomical Databases, operated at CDS, Strasbourg, France (http://cdsweb.u-strasbg.fr/), and of NASAs Astrophysics Data System, of the Jean-Marie Mariotti Center Search service (http://www.jmmc.fr/searchcal), co-developed by FIZEAU and LAOG/IPAG.

REFERENCES

Adams J. D., Stauffer J. R., Monet D. G., Skrutskie M. F., Beichman C. A., 2001, AJ, 121, 2053
Aldering G. et al., 2002, in Tyson J. A., Wolff S., eds, Proc. SPIE Conf. Ser. Vol. 4836, Survey and Other Telescope Technologies and Discoveries. SPIE, Bellingham, p. 61
Ansdell M. et al., 2015, ApJ, 798, 41
Barnes S. A., 2007, ApJ, 669, 1167
Bianchi L., 2014, Ap&SS, 354, 103
Bianchi L., Herald J., Efremova B., Girardi L., Zabot A., Marigo P., Conti A., Shiao B., 2011, Ap&SS, 335, 161
Boyajian T. S. et al., 2012, ApJ, 757, 112
Boyajian T. et al., 2015, MNRAS, 447, 846
Bressan A., Marigo P., Girardi L., Salasnich B., Dal Cero C., Rubele S., Nanni A., 2012, MNRAS, 427, 127
Casewell S. L., Dobbie P. D., Hodgkin S. T., Moraux E., Jameson R. F., Hambly N. C., Irwin J., Lodieu N., 2007, MNRAS, 378, 1131
Chaboyer B., Demarque P., Pinsonneault M. H., 1995, ApJ, 441, 876
Claret A., Bloemen S., 2011, A&A, 529, A75
Coşkunoğlu B. et al., 2011, MNRAS, 412, 1237
Crossfield I. J. M. et al., 2016, ApJS, 226, 7
Cushing M. C., Vacca W. D., Rayner J. T., 2004, PASP, 116, 362
Dahm S. E., 2015, ApJ, 813, 108
David T. J. et al., 2016, AJ, 151, 112
Dotter A., Chaboyer B., Jevremović D., Kostov V., Baron E., Ferguson J. W., 2008, ApJS, 178, 89
Dressing C. D., Charbonneau D., 2015, ApJ, 807, 45
Feast M., Whitelock P., 1997, MNRAS, 291, 683
Feiden G. A., 2016, A&A, 593, 99
Feiden G. A., Chaboyer B., 2013, ApJ, 779, 183
Findeisen K., Hillenbrand L., Soderblom D., 2011, AJ, 142, 23
Foreman-Mackey D., Hogg D. W., Lang D., Goodman J., 2013, PASP, 125, 306
Fortney J. J., Ikoma M., Nettelmann N., Guillot T., Marley M. S., 2011, ApJ, 729, 32
Funayama H., Itoh Y., Oasa Y., Toyota E., Hashimoto O., Mukai T., 2009, PASJ, 61, 931
Gaidos E., Mann A. W., 2013, ApJ, 762, 41
Gaidos E. et al., 2014, MNRAS, 443, 2561
Gaidos E., Mann A. W., Kraus A. L., Ireland M., 2016a, MNRAS, 457, 2877
Gaidos E., Mann A. W., Ansdell M., 2016b, ApJ, 817, 50
Geffert M., Kuemmel M. W., Schmidt H., 1995, A&AS, 112, 229
Gelman A., Rubin D., 1992, Stat. Sci., 7, 457
Gomes R., Levison H. F., Tsiganis K., Morbidelli A., 2005, Nature, 435, 466
Guillot T., Gautier D., 2014, preprint (arXiv:1405.3752)
Guthrie B. N. G., 1987, Q. J. R. Astron. Soc., 28, 289
Hartman J. D., Bakos G. Á., Kovács G., Noyes R. W., 2010, MNRAS, 408, 475
Henden A. A., Levine S. E., Terrell D., Smith T. C., Welch D., 2012, J. Am. Assoc. Var. Star Obs., 40, 430
Henry T. J., McCarthy Jr, D. W., 1993, AJ, 106, 773
Hirano T., Sanchis-Ojeda R., Takeda Y., Winn J. N., Narita N., Takahashi Y. H., 2014, ApJ, 783, 9
Howard A. W. et al., 2012, ApJS, 201, 15
Huber D. et al., 2016, ApJS, 224, 2
Husser T.-O., Wende-von Berg S., Dreizler S., Homeier D., Reiners A., Barman T., Hauschildt P. H., 2013, A&A, 553, A6
Kipping D. M., 2010, MNRAS, 408, 1758
Kipping D. M., 2013, MNRAS, 435, 2152
Kovács G., Zucker S., Mazeh T., 2002, A&A, 391, 369
Kraus A. L., Ireland M. J., Martinache F., Lloyd J. P., 2008, ApJ, 679, 762
Kraus A. L., Shkolnik E. L., Allers K. N., Liu M. C., 2014, AJ, 147, 146
Kreidberg L., 2015, PASP, 127, 1161
Lantz B. et al., 2004, in Mazuray L., Rogers P. J., Wartmann R., eds, Proc. SPIEConf. Ser. Vol. 5249, Optical Design and Engineering. SPIE, Bellingham, p. 146
Lee J.-J., 2015, plp: Version 2.0. Available at: (http://dx.doi.org/10.5281/zenodo.18579)
Li C., Junliang Z., 1999, in Egret D., Heck A., eds, ASP Conf. Ser. Vol. 167, Harmonizing Cosmic Distance Scales in a Post-HIPPARCOS Era. Astron. Soc. Pac., San Francisco, p. 259
Lind K., Asplund M., Barklem P. S., 2009, A&A, 503, 541
Luhman K. L., Stauffer J. R., Mamajek E. E., 2005, ApJ, 628, L69
McCarthy K., Wilhelm R. J., 2014, AJ, 148, 70
McQuillan A., Aigrain S., Mazeh T., 2013, MNRAS, 432, 1203
Makarov V. V., Robichon N., 2001, A&A, 368, 873
Mamajek E. E., Hillenbrand L. A., 2008, ApJ, 687, 1264
Mandel K., Agol E., 2002, ApJ, 580, L171
Mann A. W., von Braun K., 2015, PASP, 127, 102
Mann A. W., Feiden G. A., Gaidos E., Boyajian T., von Braun K., 2015, ApJ, 804, 64
Mann A. W. et al., 2016a, ApJ, 152, 61
Mann A. W. et al., 2016b, ApJ, 818, 46
Marchwinski R. C., Mahadevan S., Robertson P., Ramsey L., Harder J., 2015, ApJ, 798, 63

Markwardt C. B., 2009, in Bohlender D. A., Durand D., Dowler P., eds, ASP Conf. Ser. Vol. 411, Astronomical Data Analysis Software and Systems XVIII. Astron. Soc. Pac., San Francisco, p. 251
Melis C., Reid M. J., Mioduszewski A. J., Stauffer J. R., Bower G. C., 2014, Sci, 345, 1029
Metchev S. A., Hillenbrand L. A., 2009, ApJS, 181, 62
Monet D. G. et al., 2003, AJ, 125, 984
Morrissey P. et al., 2007, ApJS, 173, 682
Morton D. C., 1991, ApJS, 77, 119
Morton T. D., Swift J., 2014, ApJ, 791, 10
Mulders G. D., Pascucci I., Apai D., 2015, ApJ, 798, 112
Nordström B. et al., 2004, A&A, 418, 989
Ortega V. G., Jilinski E., de La Reza R., Bazzanella B., 2007, MNRAS, 377, 441
Park C. et al., 2014, Proc. SPIE, 9147, 91471D
Parviainen H., Aigrain S., 2015, MNRAS, 453, 3821
Pepe F. et al., 2014, Astron. Nachr., 335, 8
Petigura E. A., Howard A. W., Marcy G. W., 2013, Proc. Natl. Acad. Sci., 110, 19273
Queloz D., Allain S., Mermilliod J.-C., Bouvier J., Mayor M., 1998, A&A, 335, 183
Rauer H. et al., 2014, Exp. Astron., 38, 249
Rayner J. T., Toomey D. W., Onaka P. M., Denault A. J., Stahlberger W. E., Vacca W. D., Cushing M. C., Wang S., 2003, PASP, 115, 362
Rebull L. M. et al., 2016, preprint (arXiv:1606.00052)
Reid I. N., Cruz K. L., 2002, AJ, 123, 2806
Reinhold T., Reiners A., Basri G., 2013, A&A, 560, A4
Ricker G. R. et al., 2014, in Oschmann J. M., Jr, Clampin M., Fazio G. G., MacEwen H. A., eds, Proc. SPIE Conf. Ser. Vol. 9143, Space Telescopes and Instrumentation 2014: Optical, Infrared, and Millimeter Wave. SPIE, Bellingham, p. 914320
Rizzuto A. C., Ireland M. J., Robertson J. G., 2011, MNRAS, 416, 3108
Rizzuto A. C., Ireland M. J., Kraus A. L., 2015, MNRAS, 448, 2737
Rogers L. A., 2015, ApJ, 801, 41
Róser S., Demleitner M., Schilbach E., 2010, AJ, 139, 2440
Röser S., Schilbach E., Piskunov A. E., Kharchenko N. V., Scholz R.-D., 2011, A&A, 531, A92
Sarro L. M. et al., 2014, A&A, 563, A45
Scargle J. D., 1982, ApJ, 263, 835
Silburt A., Gaidos E., Wu Y., 2015, ApJ, 799, 180
Skrutskie M. F. et al., 2006, AJ, 131, 1163
Soderblom D. R., Stauffer J. R., Hudon J. D., Jones B. F., 1993, ApJS, 85, 315
Soderblom D. R., Laskar T., Valenti J. A., Stauffer J. R., Rebull L. M., 2009, AJ, 138, 1292
Somers G., Pinsonneault M. H., 2014, ApJ, 790, 72
Somers G., Pinsonneault M. H., 2015, MNRAS, 449, 4131
Stauffer J. R. et al., 2007, ApJS, 172, 663
Stauffer J. R. et al., 2016, preprint (arXiv:1606.00057)
Swift D. C. et al., 2012, ApJ, 744, 59
Takeda Y., Ohkubo M., Sadakane K., 2002, PASJ, 54, 451
Thommes E., Nagasawa M., Lin D. N. C., 2008, ApJ, 676, 728
Tian F., Toon O. B., Pavlov A. A., De Sterck H., 2005, ApJ, 621, 1049
Tuthill P. G., Monnier J. D., Danchi W. C., 2000, in Léna P., Quirrenbach A., eds, Proc. SPIE Vol. 4006, Interferometry in Optical Astonomy. SPIE, Bellingham, p. 491
Tukey J. W., 1977, Exploratory Data Analysis. Addison-Wesley, Reading, MA
Vacca W. D., Cushing M. C., Rayner J. T., 2003, PASP, 115, 389
van Leeuwen F., 2009, A&A, 497, 209
Vanderburg A., Johnson J. A., 2014, PASP, 126, 948
Vanderburg A. et al., 2016, ApJS, 222, 14
Volk K., Gladman B., 2015, ApJ, 806, L26
Weiss L. M., Marcy G. W., 2014, ApJ, 783, L6
White R. J., Gabor J. M., Hillenbrand L. A., 2007, AJ, 133, 2524
Yuan H. B., Liu X. W., Xiang M. S., 2013, MNRAS, 430, 2188
Zacharias N., Finch C. T., Girard T. M., Henden A., Bartlett J. L., Monet D. G., Zacharias M. I., 2013, AJ, 145, 44
Zapatero Osorio M. R. et al., 2014, A&A, 568, A77

This paper has been typeset from a TEX/LATEX file prepared by the author.